Simultaneous Transfer Path Analysis of Axial Piston Pump Lumped Parameter Model Results

Dazhuang He[1], Antonio Masia[2], Yangfan Liu[3], Lizhi Shang[4], Daniel Dyminski[5]

[1] Ray W. Herrick Laboratories, Purdue University. 177 S Russell St, West Lafayette, IN 47907, USA. he385@purdue.edu

[2] Department of Agricultural & Biological Engineering, Purdue University Maha Fluid Power Research Center 1500 Kepner Drive, Lafayette, IN 47905 USA. amasia@purdue.edu

[3] Assistant Professor of Mechanical Engineering, Ray W. Herrick Laboratories, Purdue University. 177 S Russell St, West Lafayette, IN 47907, USA. yangfan@purdue.edu

[4] Assistant Professor of Mechanical Engineering and Agricultural & Biological Engineering, Purdue University Maha Fluid Power Research Center 1500 Kepner Drive, Lafayette, IN 47905 USA. shangl@purdue.edu

5 Principal Engineer, Hydraulic Pump and Power System Division Parker Hannifin Corporation. daniel.dyminski@parker.com

Abstract.

The recent trend in electrifying off-road vehicles has brought to light a critical issue – the noise emission of hydrostatic pumps and motors. In the transition from internal combustion engines (ICE) to electric motors, the previously masked noise from hydraulic pumps and motors has become significant in fluid power systems for off-road applications. The purpose of present study is to develop a analyzing tool of noise and vibration of hydrostatic pumps and motors. To achieve this goal, a dedicated lumped parameter model (LPM) was developed in Amesim. The numerical model takes into account various factors, including the fluid-dynamic path, unit kinematics, forces and moments acting on the main components. The lumped parameter model simulates the internal forces/moments/ripples that cause noise and vibration of the axial piston pump. The method of simultaneous transfer path analysis (sTPA) is then applied to the relation between internal forces/moments/ripples and consequent noise and vibration.

With simultaneous excitation information provided by LPM and operational measurement of acoustic/vibration responses, sTPA estimates the frequency response functions between the excitations and acoustical/vibrational responses. Path contribution information provided by sTPA characterizes the significance of individual transfer paths. A 45cc pump was subjected to testing enabling the collection of data of noise levels, vibrations and flow ripples over a large range of operating conditions. With both measurement and simulation results, sTPA is conducted to analyze how the pump internal excitations (forces, moments and ripples) correlate with pump noise and vibration. The results provided by sTPA highlights the critical path contributions and the main mechanisms that contribute to the noise emission

over a range of frequencies. A parameter sensitivity analysis based on sTPA results is conducted, in which the sensitivities of noise and vibration level of the piston pump to multiple design/operation parameters are investigated. In the case study, sTPA reveals that the moment oscillation exerted on the pump has the most significant impact on the overall vibration level, and the bearing force oscillation has the most significant impact on the overall noise level. In conclusion, sTPA is a tool that bridges the gap between LPM calculation results and air-borne noise/vibration performance of hydraulic pumps and provides insights to the root-cause of noise and vibration problems of axial piston pumps.

Keywords. Transfer path analysis, lumped parameter model, axial piston pump.

1. INTRODUCTION

Axial piston pumps are widely used in applications such as agricultural, construction and industrial vehicles. Due to the pulsive nature of the working principles of axial piston pumps, oscillatory forces, moments and pressure ripples are major sources of noise and vibration during the operation of piston units. In recent years, trend of electrification of off-road vehicles poses new challenges for the mitigation of noise and vibration of hydraulic units, because the quieter electrical powertrain accentuates the noise emitted from hydraulic units, which are otherwise masked by the noise from conventional ICE powertrain.

Despite the noise, vibration and harshness (NVH) performance of hydraulic pump/motor has been vastly improved over the course of fluid power technology development, the problem of noise and vibration generation remains a challenge. Specifically, the noise and vibration issue are more prominent for piston machines than gear or screw machine [1] due to its pulsive nature. Early efforts of noise reduction for piston machines focused mainly on *structure borne noise* (SBN) mainly induced by vibration of pump/motor components. Helgested *et al*. studied the effect of rate of pressurization on pump casing vibration and noise [2]. Yamauchi *et al*. investigated how factors such as pressurization rate, relief groove and dead volume affects swash plate vibration in piston pumps [3]. Kim and Ivantysynova designed a pump control system, in which an anti-moment is actively exerted on the swashplate to reduce its vibration [4]. *Fluid borne noise* (FBN) stem from the pressure and flow pulsations. As a result, the mitigation measures for FBN mainly focus on the reduction of flow/pressure ripples. Harrison *et al.* developed valve plates with a heavily damped check valve ahead of delivery port to reduce the flow ripple [5]. Ortwig installed a silencer in hydraulic circuit to reduce pulsations propagating through the hydraulic line [6]. Rebel attempted to introduce anti-noise, i.e., secondary pressure ripples that destructively interfere with the original ripples, to reduce FBN [7]. Techniques of FBN reduction has been comprehensively summarized by Harrison *et al.* [5].

In the aforementioned studies about noise reduction measures of piston pumps, the goal researchers attempted to achieve is always the reduction of pump internal force/moment/ripples. However, the oscillatory excitations, either structure borne or fluid borne, transmit differently through multiple paths and contribute to the noise level at designated locations, e.g., vehicle operator's ears. In order to conduct a thorough root-cause analysis for noise and vibration of piston units, a quantitative approach that correlates the internal excitations and perceivable noise and vibration of the pump is necessary. Such approach reveals how sources of noise and vibration transmit via different transfer paths. For this purpose, the method of simultaneous transfer path analysis (sTPA) is developed in

the present study and applied to piston units with internal excitations generated by a lumped parameter model (LPM) of axial piston pump.

LPM has been proven to be a reliable method to capture the internal force, moments and ripples of hydraulic units. In the work proposed by Manco *et al.*, [8] and [9] a lumped parameter model has been developed, showing remarkable agreement between simulation and measurements. A similar numerical model is available as a built-in component in the software Amesim. In the present study, a dedicated lumped parameter model is developed in Amesim to overcome the constraints of an imposed model, allowing the author the flexibility to access the source code to model the components that are the focus of interest for this study, which are not available in the current state of the art models. The numerical model takes into account the fluid-dynamic path, the unit kinematics and dynamics, and the forces and moments that are exerted on the main components, in particular, the forces and moments exerted on the port case of the pumps.

The conceptual LPM+sTPA framework is shown in the diagram in **Figure 1**. The pump sound and vibration measurement are carried out for multiple operation conditions, and LPM simulation is also conducted for the same operation conditions. sTPA is the processing tool for both the sound and vibration response data acquired in measurement and internal excitations data simulated using LPM. By feeding sTPA the excitation and response data for multiple operation conditions, sTPA estimates frequency response functions (FRFs) that characterize the transfer paths between excitation and response.

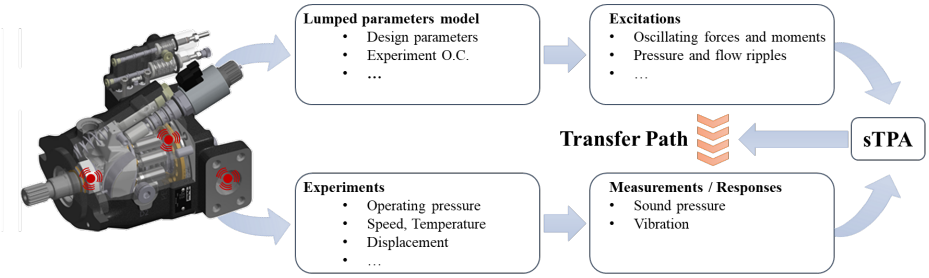

Figure 1 LPM+sTPA framework

Coupling LPM with sTPA has advantages in noise/vibration mitigation of pumps. sTPA requires simultaneous data of internal excitation, and LPM provides high fidelity data of internal excitations which is otherwise difficult to measure. With sTPA, the reductions in internal forces/moments/ripples can be quantified in terms of noise/vibration levels reductions. sTPA not only fills the gap between internal excitations and consequent noise/vibration level, but also provides guidelines on noise/vibration mitigation of the pump. By inspecting the FRF and path contributions, one can identify the critical paths. Once the critical paths are identified, noise/vibration mitigation measures can be explored using the estimated FRFs.

In this paper, the development of piston unit LPM is covered in the chapter 2. The methodology of sTPA is introduced in chapter 3. The results of transfer path FRF and path contributions are shown in chapter 4. Conclusions of the study is presented in the chapter 5.

2. LUMPED PARAMETER MODEL FOR PISTON UNIT

The mathematical model for simulating axial piston pump swashplate type is described in detail in this section. The model allows for the evaluation of the unit performance under both steady-state and dynamic conditions. It has been designed and implemented to be parametric, which means that it provides the flexibility to vary the geometric parameters of a unit or a specific feature and see their effects on the performances compared to a baseline design. **Figure 2** shows the cross-sectional view of an axial piston machine swashplate type with the main components considered for the model implementation labelled.

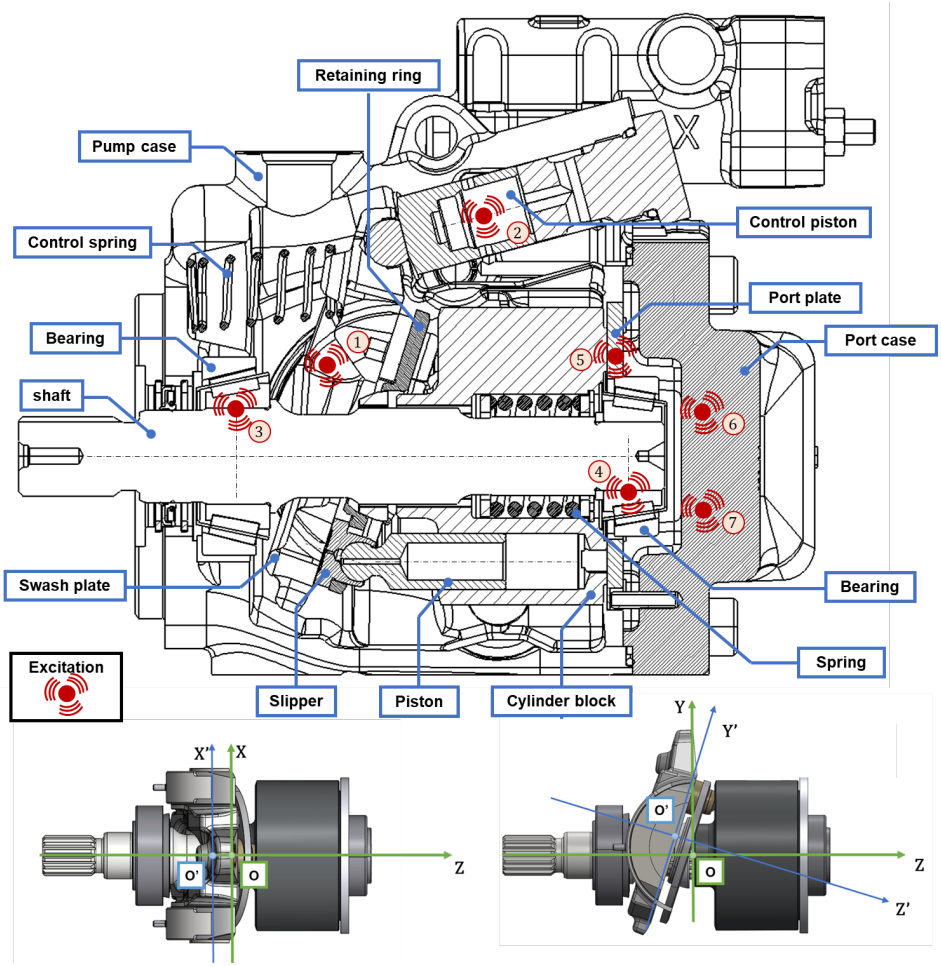

Figure 2 Axial piston pump cross-section and reference system

Two reference systems were selected. A fixed cartesian coordinate system is considered center at the center of the instantaneous rotation of the swashplate and a mobile coordinate system is considered center on the swashplate. The eccentricity of the swashplate is considered a design parameter as well. In **Figure 2** shows the main point that represents source of excitation that contribute to noise generation. Internal forces and moments have the potential to excite the pump housing, resulting in the pump vibration which results in

air-borne noise. The excitation includes ① the force from the swashplate, ② the pressure ripple in the swashplate control cylinder, ③ & ④ the force from the shaft through the two bearings, ⑤ the force on the port case from the cylinder block, and ⑥ & ⑦ the pressure ripples in the inlet and outlet port of the unit. In this study, the focus is only on ④, ⑤ which represents the excitation that most affects the port case of the pump. The swashplate force and the bearing force ③ are not considered because they are located next to the mounting interface where due to the rigid connection the housing is not free to deform. The pressure ripple in the swashplate control system is neglected because relatively low. The pressure ripple in the inlet and outlet port will results in more fluid-born noise, but limited air-borne.

2.1. Fluid Dynamic Model

To model the fluid dynamic behaviour of the unit, a lumped parameter method has been chosen. The first step is to discretize the unit into its equivalent fluid dynamic block diagram, shown in **Figure 3**. Where the entire pump fluid dynamic system is represented as a set of discrete components each characterized by lumped parameters such as volume, pressure, and flow rate. For simplicity is assumed that the unit is working in pumping mode, and the flow flows from left to right.

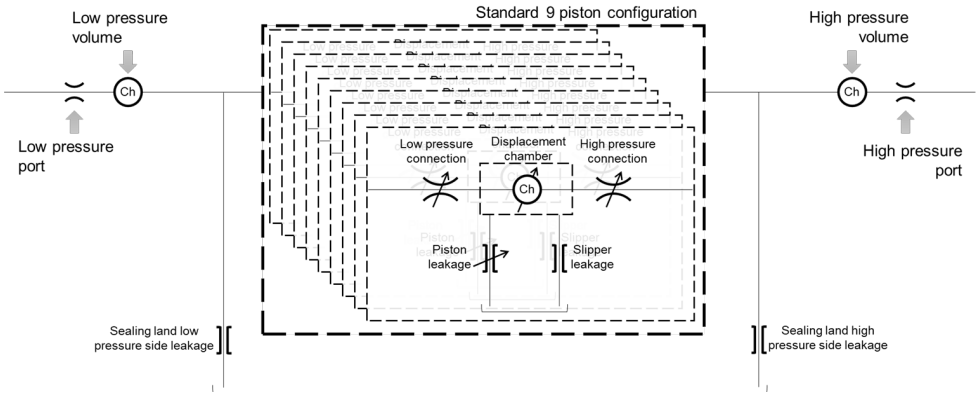

Figure 3 Axial piston pump fluid-dynamic block diagram.

To model the fluid dynamics within the axial piston machine, it is essential to analyse both its kinematic behaviour and the influence of component motion on the fluid path.

An axial piston pump typically features two ports: one for suction and one for delivery. In the pumping mode, the suction port operates at low pressure while the delivery port operates at high pressure. A fixed orifice is selected to model the ports, while a fixed volume is chosen to simulate the dead volume that is present inside the port-case. The structure of the pump's rotary group includes: shaft, cylinder block, pistons, and slippers. Traditionally, swashplate-type units feature configurations with nine pistons. During a single shaft revolution, each piston performs two primary actions: suction and delivery. In the suction phase, the piston moves out from the displacement chamber, allowing fluid to enter. In the delivery phase, the piston moves into the displacement chamber, pushing the fluid out. This process is repeated every shaft revolution, with the piston communicating with the low-pressure side during suction and the high-pressure side during delivery. A variable orifice is employed to model the opening and closing between the low and high-pressure sides of the pump.

The equation representing a variable orifice is the orifice equation, which can be expressed as follows:

$$Q_i = c_d \cdot A_i \cdot \sqrt{\frac{2 \cdot \Delta p}{\rho}} \tag{1}$$

The subscript "i" in the equation generalizes its form to a vectorial representation, where the "i" element corresponds to the "i-th" piston. A_i is the effective flow area for each piston. Its profile during a single revolution is crucial for replicating the proper behavior of the unit. The area profile depends on the design of the valve plate shown in **Figure 4**, which regulates the timing for connecting the displacement chamber with the low and high pressure.

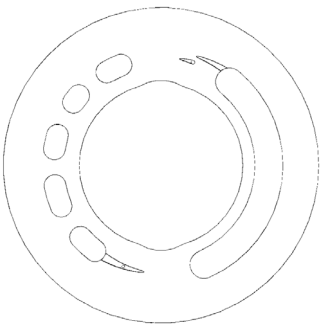

Figure 4 Valve plate

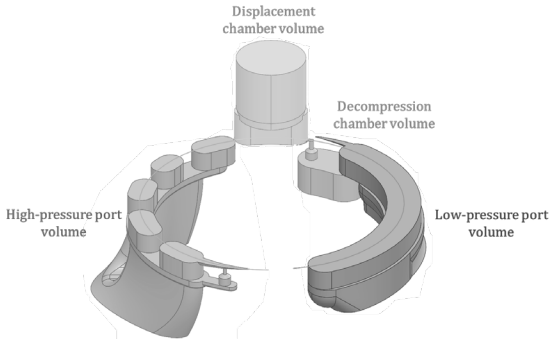

Figure 5 Fluid volume analysis

To evaluate the area profile, the AVAS toll was used. AVAS, expanded as Automated Valve Plate Area Search, is an in-house software that solves for a minimum area of cross-section of the fluid geometry (shown in **Figure 5**) normal to the flow streamline for every desired step angle in a shaft revolution. This area is the smallest opening between the cylinder clock and the valve plate in the direction of flow between the displacement chamber and the high-pressure or low-pressure ports.

The pressure within the displacement chamber changes and these variations can be described by the pressure build-up equation.

$$\frac{dp}{dt} = \frac{\beta}{V} \cdot \left(Q_{in} - Q_{out} - \frac{dV}{dt} \right) \tag{2}$$

This equation represents the instantaneous relationship that connects the pressure variation in the chamber to the sum of the flows and the volume variation It is also essential to consider the leakages from the three main lubricating interfaces. These leakages are approximated considering a laminar flow, with a constant gap height and with a linear or exponential pressure gradient. The laminar flow approximation, characterized by low Reynold number, simplifies its complexity making it suitable for a lumped parameter approach. The model considers the three main lubricating interfaces as a laminar interface with a constant gap height and their expression can be found analytically [10].

2.2. Mechanical Model

This section presents a simplified study of the mechanical components of the axial piston unit. For each individual component, equilibrium equations for translation and rotation were developed, allowing the evaluation of the forces and moments exerted on a single component. The reference coordinate systems and nomenclature of the main geometric points that define the motion of the pistons and slippers are shown in **Figure 2**. A free-body diagram approach has been used to define the equations that describe the kinematics and dynamics of the main elements. Particular attention was focused on the port case.

2.2.1. Port case

The displacement chamber exerts a pressure force acting against the cylinder block. This force is then transferred to the port case via the valve plate. A thorough evaluation of the equilibrium of forces and moments is performed to determine which component may be influencing the noise emission of the hydraulic machine. The valve plate is considered to be simplified to a two-dimensional plane. **Figure 6** shows how a reference system is set up in the center of the port case.

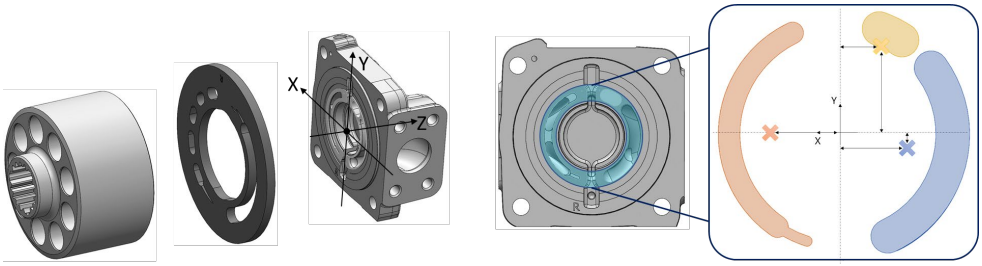

Figure 6 Port case notation

$$F_{pc} = \sum_{i=1}^{Np} -F_{p,i} + F_{vp} \tag{4}$$

Where F_{pc} represent the force applied on the port case, $F_{p,i}$ is the pressure force from the displacement chamber, and F_{vp} is the force from the valve plate. The force exerted by the valve plate is evaluated using three pressure values: low pressure, high pressure, and pressure within the inlet baffle chamber (Patent applied EP347171A1). Each of these pressures, multiplied by their corresponding area (as shown in **Figure 6**), produces a force opposite to the one generated by the cylinder block. The resulting force F_{pc} is expected to transfer to the port case. A three-dimensional computer-aided design (3D-CAD) study was used to determine the center of each region, resulting in coordinate coordinates relative to the x and y axes. A study of the moments operating on the port case was done assuming that the force generated by each area would is applied to its geometrical center.

$$M_{pc,x} = \sum_{i=1}^{Np} -F_{p,i} \cdot y_{p,i} + M_{vp,x} \tag{4}$$

Where $M_{pc,x}$ is the moment acting on the port case around the x-axis. A similar approach has been applied to determine the moment around the y-axis $M_{pc,y}$.

Another excitation to consider for the sTPA is the bearing force. The cylinder block and the shaft are assumed to be rigidly connected through a splined interface. The midpoint of the spline serves as the reference point. Using this reference, the force exerted by the cylinder block and the bearing location are employed to evaluate the force exerted on the bearing.

2.3. Experimental investigation and model validation

To validate the lumped parameter model, a series of experiments were run under steady-state conditions. These tests were primarily designed to measure the pressure ripple at 'he pump's outlet port. The experimental data were then compared to the simulated results generated by the model. The comparison aimed to evaluate the model's accuracy. The following **Figure 7** depicts the hydraulic schematic used for the experiments for model validation.

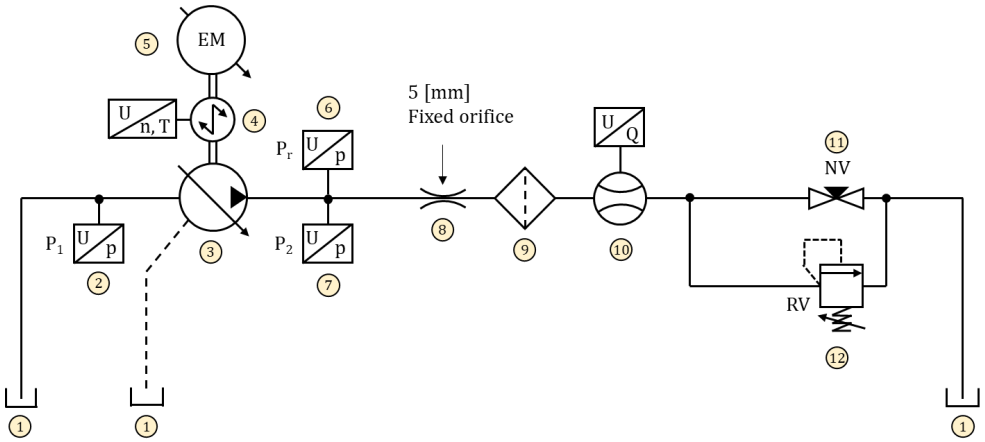

Figure 7 Hydraulic schematic.

A standard reservoir ① is connected to the unit under testing ③, which is driven by an electric motor ⑤. A torque meter ④ is used to monitor speed and torque. Two pressure sensors ② and ⑦ measure pressure differential throughout the unit, while a piezoelectric transducer ⑥ measures pressure ripple. The pump load is regulated by a fixed orifice ⑧, which is connected to the pressure sensors ⑥, ⑦ via a rigid pipe. Following the opening, a high-pressure filter ⑨ comes before the flow meter ⑩. Next, a needle valve ⑪ is added to regulate pump load. For safety, a pressure relief valve ⑫ is connected in parallel.

The tests analysed the hydraulic unit's performance at various operating speeds and pressure levels. The unit was operated at 1000, 1500, 2000 rpm, and 2500 rpm. The pressure within the system was monitored at each speed increment, with the needle valve fully open serving as the baseline. The pressure levels obtained by adjusting the needle valve opening to reach 75, 125, and 175 bar offered insight into the unit behavior across the speed range, assisting in the validation and calibration of the lumped parameter model.A series of custom components were developed to create a comprehensive library of components, which were then integrated into the Amesim environment. This new library contains customized

components modeled according to physical principles, with parametric and vectorial properties, including the parameter for the number of pistons. To consider the loading condition, the model use standard components already present in the Amesim library for modeling the rigid pipe and the orifice. Then, it is assumed that the pressure ripple is affected by orifice pressure drop, so a pressurized tank is used to generate the pump load. The validation of this model involves the comparison of the pressure ripple measured at the pump's outlet port. An FFT analysis was conducted on the measurements, revealing that 2000 rpm was the optimal configuration for validating the model due to its lower noise levels compared to other operating speeds. Additionally, the higher noise in the measurements might be attributed to the nonlinearity of the physical components present in the hydraulic circuit, which can be challenging to model using a lumped parameter approach. The following **Figure 8** and **Figure 9** show the comparison of the pressure ripple measured and the pressure ripple simulated.

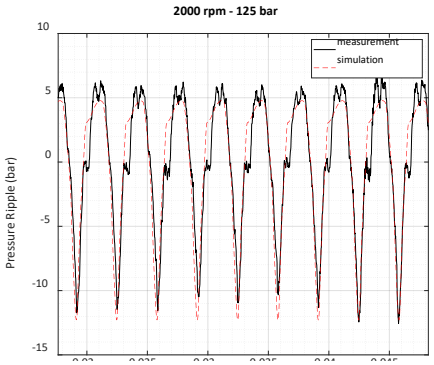

Figure 8 Sim–vs Mes - 1

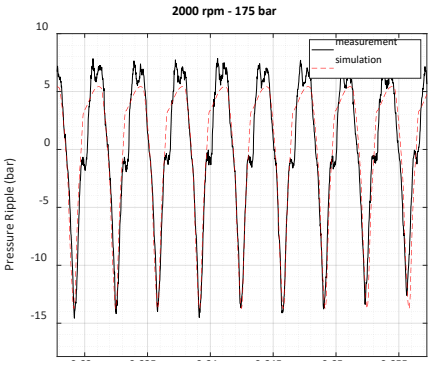

Figure 9 Sim–vs Mes - 2

As can be noticed, the model is able to capture the pressure ripple amplitude respect different level of pressure and follow the measurement profile. The comparison on the pressure ripple amplitude led to the following evaluation of the model accuracy

Speed [rpm]	**Pressure [bar]**	**Mes Δ ripple [bar]**	**Sim Δ ripple [bar]**	**Error [%]**
2000	175	20	19.14	4.30
2000	125	16	17	6.25
2000	75	13.5	14.3	5.93

The results show that the model can simulate the pressure ripple with an average error of 5.5% with respect the measurement results.

3. SIMULTANEOUS TRANSFER PATH ANALYSIS

Transfer path analysis (TPA) is a technique used to break down noise or vibration into its key contributors. The noise/vibration contributors are characterized using frequency response functions from excitations to the acoustic/vibration responses at target locations.

The three major components in the TPA calculation are:

- Excitations: The spectrum of forces/moments source that causes noise and vibration.
- Responses: The noise/vibration acquired at target locations.
- Transfer Paths: The mathematical relation that characterizes how noise and vibration are transferred from source excitation to the responses.

Figure 10 shows the relation of excitations, responses and the transfer paths in between for a mechanical system with 3 excitations, 2 responses and 6 transfer paths. In general, if there are r excitations and m responses, the number of transfer paths is r-by-m. The task of TPA is to determine the frequency response functions (transfer functions) for each transfer path mathematically.

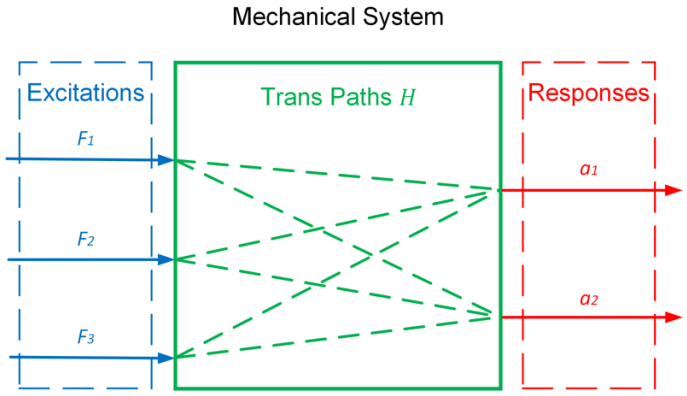

Figure 10 Excitations, responses and transfer paths in TPA

TPA has been a widely used engineering tool for the analysis of mechanical vibration transmissions for a variety of industrial products, and the methodologies of TPA has kept developing over time. Van der Seijs *et al*. provides a compressive review on the landscape of TPA methods [11]. In the conventional practice of TPA, the excitations are isolated and applied to the mechanical system individually. In the example shown in Figure 10, if excitation $\boldsymbol{F_1}$ is isolated and applied, then the frequency response function from $\boldsymbol{F_1}$ to responses $\boldsymbol{a_1}$ and $\boldsymbol{a_1}$ can be simply calculated as $\boldsymbol{H_{11} = a_1/F_1}$ and $\boldsymbol{H_{21} = a_2/F_1}$.

However, for axial piston pumps, it is difficult to isolate excitations and apply them individually. For example, in an operating hydraulic pump, the oscillatory fluid pressure ripples cause noise and vibration, yet it is difficult to investigate the fluid pressure related transfer path alone, without introducing other *simultaneous* excitations such as the bearing force due to pressure imbalance across cylinders. For this reason, a sub-category of TPA methodology, simultaneous TPA (sTPA, also referred to as operational TPA), is thus more suitable for the estimation of transfer path FRFs for such mechanical systems. sTPA has

gained popularity in multiple engineering areas as a NVH analysis tool [12-15], due to its ease to setup the measurement. Instead of isolating and applying excitations individually, in the practice of sTPA, multiple independent combinations of operational excitations are created by altering the operation conditions of the mechanical system. Assume the system is tested under n operation conditions, the mathematical relation of excitations, responses and transfer paths can be cast in a matrix form:

$$\begin{bmatrix} a_1^{(1)} & a_1^{(2)} & \cdots & a_1^{(n)} \\ a_2^{(1)} & a_2^{(2)} & \cdots & a_2^{(n)} \\ \vdots & \vdots & \ddots & \vdots \\ a_m^{(1)} & a_m^{(2)} & \cdots & a_m^{(n)} \end{bmatrix}_{m\times n} = \begin{bmatrix} H_{11} & H_{12} & \cdots & H_{1r} \\ H_{21} & H_{22} & \cdots & H_{2r} \\ \vdots & \vdots & \ddots & \vdots \\ H_{m1} & H_{m2} & \cdots & H_{mr} \end{bmatrix}_{m\times r} \begin{bmatrix} F_1^{(1)} & F_1^{(2)} & \cdots & F_1^{(n)} \\ F_2^{(1)} & F_2^{(2)} & \cdots & F_2^{(n)} \\ \vdots & \vdots & \ddots & \vdots \\ F_r^{(1)} & F_r^{(2)} & \cdots & F_r^{(n)} \end{bmatrix}_{r\times n} \tag{5}$$

$$[a]_{m\times n} = [H]_{m\times r}[F]_{r\times n} \tag{6}$$

in which $\boldsymbol{a_i^{(k)}}$ represents the i-th response at the k-th operation condition, $\boldsymbol{F_j^{(k)}}$ represents the j-th excitation at the k-th operation condition, and $\boldsymbol{H_{ij}}$ is the ratio of $\boldsymbol{a_i}$ to $\boldsymbol{F_j}$. For piston pumps, $\boldsymbol{a_i}$ can be responses that characterize noise/vibration of the unit, such as sound pressure or pump housing vibration acceleration. $\boldsymbol{F_j}$ can be variables such as pressure/flow ripples or bearing forces, which characterize noise/vibration inducing mechanisms of the pump. In sTPA, $\boldsymbol{a_i^{(k)}}$ is a frequency-dependent matrix containing responses such as sound acceleration, velocity or sound pressure, acquired by sound/vibration test. $\boldsymbol{F_j^{(k)}}$ is a frequency dependent matrix acquired from LPM simulation that contains the source magnitude and phase. The independence of excitations can be verified by stacking matrix $\boldsymbol{F_j^{(k)}}$ of different frequencies row-wise and calculating the rank of the stacked matrix. A rank equal to $\boldsymbol{r}$ indicates mutually independent operational excitations.

Given $\boldsymbol{a_i^{(k)}}$ and $\boldsymbol{F_j^{(k)}}$, the i-th row of $[\boldsymbol{H}]$ be estimated as

$$\begin{Bmatrix} H_{i1} \\ H_{i2} \\ \vdots \\ H_{ir} \end{Bmatrix} = ([A]^H[A])^{-1}[A]^H \begin{Bmatrix} a_i^{(1)} \\ a_i^{(2)} \\ \vdots \\ a_i^{(n)} \end{Bmatrix} \tag{7}$$

in which $[A] = [F]^T$. It should be noted that for equation (7) to be valid, the number of operation condition n needs to be greater than or equal to the number of excitations r.

Equation (7) provides a least-square estimate of $\{\mathbf{x}\}_i = [H_{i1} \quad H_{i2} \quad \dots \quad H_{ir}]^T$, such that norm $\|[A]\{\mathbf{x}\}_i - \{\mathbf{b}\}_i\|_2{}^2$ is minimized, in which $\{\mathbf{b}\}_i = \left[a_i^{(1)} \quad a_i^{(2)} \quad \dots \quad a_i^{(n)}\right]^T$. Since the number of operations conditions n is larger than the number of excitations r, overfitting of the transfer path FRF can occur. In order to avoid such overfitting of FRF, a regularized least-square formulation is used to replace equation 7. The regularized least square formulation minimizes $\|[A]\{\mathbf{x}\}_i - \{\mathbf{b}\}_i\|_2{}^2 + \lambda^2\|\{\mathbf{x}\}_i\|_2{}^2$, in which λ is the parameter of regularization. λ is chosen such that generalized cross validation (GCV) function

$$G(\lambda) = \frac{\|[A]\{\mathbf{x}\}_i - \{\mathbf{b}\}_i\|_2^{\,2}}{\left(tr(I - [A]([A]^H[A] + \lambda^2 I)^{-1}[A]^H)\right)^2} \tag{8}$$

is minimized.

It should be noted that different rows of matrix $[F]$ has different units. Consequently, when the least-square formulation is evaluated, the unit system applies different weights to rows of $[F]$. To eliminate the effect of unit system of choice, a normalization process is applied to matrix $[F]$ as

$$[\widetilde{F}] = \begin{bmatrix} F_1^{(1)}/\overline{F_1} & F_1^{(2)}/\overline{F_1} & \cdots & F_1^{(n)}/\overline{F_1} \\ F_2^{(1)}/\overline{F_2} & F_2^{(2)}/\overline{F_2} & \cdots & F_2^{(n)}/\overline{F_2} \\ \vdots & \vdots & \ddots & \vdots \\ F_r^{(1)}/\overline{F_r} & F_r^{(2)}/\overline{F_r} & \cdots & F_r^{(n)}/\overline{F_r} \end{bmatrix}, \tag{9}$$

in which $\overline{\boldsymbol{F_j}}$ are average values for j-th excitation over all operation conditions. Such normalization process makes $[\boldsymbol{A}] = [\widetilde{\boldsymbol{F}}]^{\boldsymbol{T}}$ dimensionless.

The method of sTPA is validated against analytical solutions of baffled pistons. The sound field of a baffled piston can be written as

$$P(\omega) = j\omega c \frac{Qk}{2\pi r} e^{-jkr} \left[\frac{2\mathrm{J}_1(ka\sin\theta)}{ka\sin\theta}\right]. \tag{10}$$

Therefore, the analytical FRF between piston volumetric displacement and radiated sound can be simply cast as P/Q. If r pistons are operating simultaneously with volumetric displacement Q_j respectively, the resulting sound field can be calculated at field points using Equation (10). Providing r different operation conditions of pistons (In this case, operation conditions is represented by independent combos of Q_j.), the problem can be formulated as in Equation (5), and the FRF can be found by sTPA. The results demonstrate total agreement as shown in **Figure 11**.

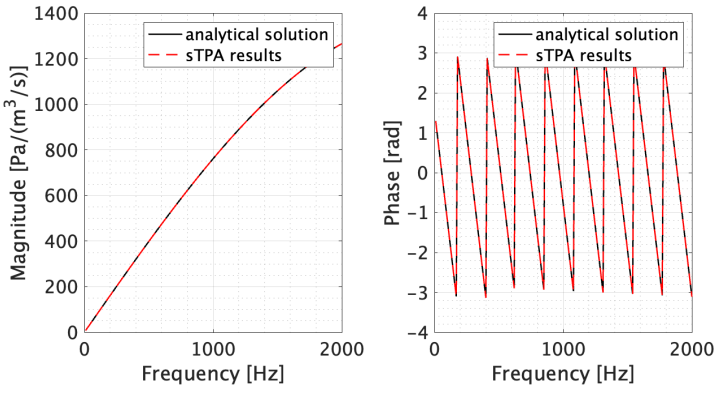

Figure 11 FRF of baffled pistons.

4. RESULTS

A 45cc pump was subjected to testing over 18 different operation conditions. The pump is set to run at a constant speed with two different configurations. Configuration A, a fixed orifice of 5 mm is located next to the outlet port of the pump, followed by a 3 m hose. In configuration B, the fixed orifice and the hose are switched in position. For both configurations, tests were run for three pressure level 50, 175, and 300 bar for three different swashplate angles, 0%, 50%, and 100%. It should be noted that the pump speed is kept constant in the case study, however, the method of sTPA is equally valid for any other pump speed.

In the pump test, two accelerations and a sound pressure are acquired. The placements of the sensors are shown in **Figure 12**. The two accelerometers measure horizontal (Z-axis) a_h acceleration and vertical (Y-axis) acceleration a_v respectively. Sound pressure p is measured 1 meter away at the same vertical level as the pump. An example of sound and vibration measurement results is shown in **Figure 13**.

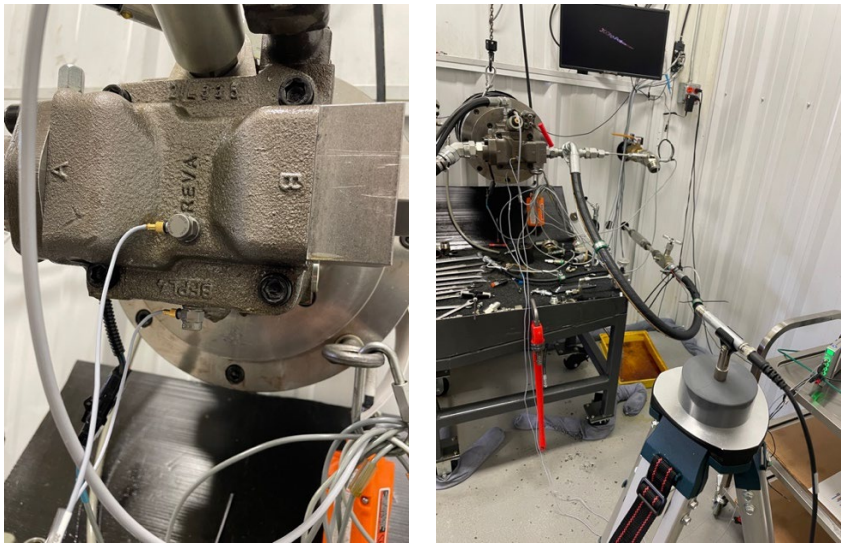

Figure 12 Sensor placement. Left: Accelerometers; Right: Microphone.

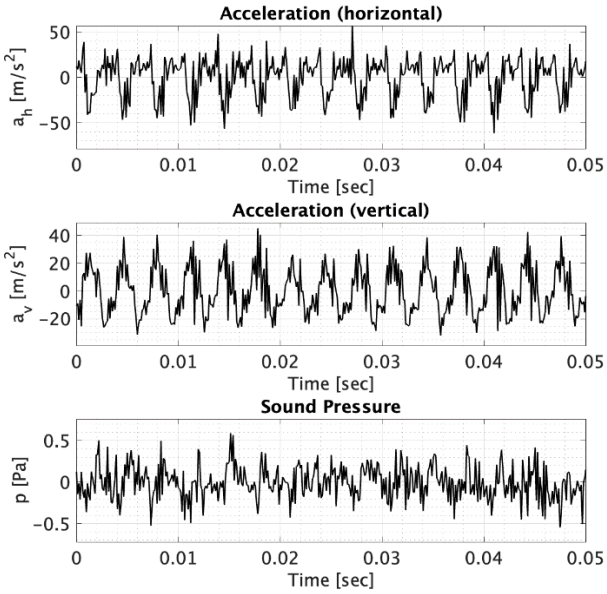

Figure 13 Noise and vibration measurement results. Operation condition: 300 bar, 50% swashplate angle, configuration B.

LPM simulations are conducted for all 18 different operation conditions. The excitations taking into consideration in present study are bearing force component in y-direction (see **Figure 6**) $F_{b,y}$, sealing land moments $M_{sl,x}$ and $M_{sl,y}$ and flow ripple Q_{out}. An example of excitation simulation results is shown in **Figure 14**.

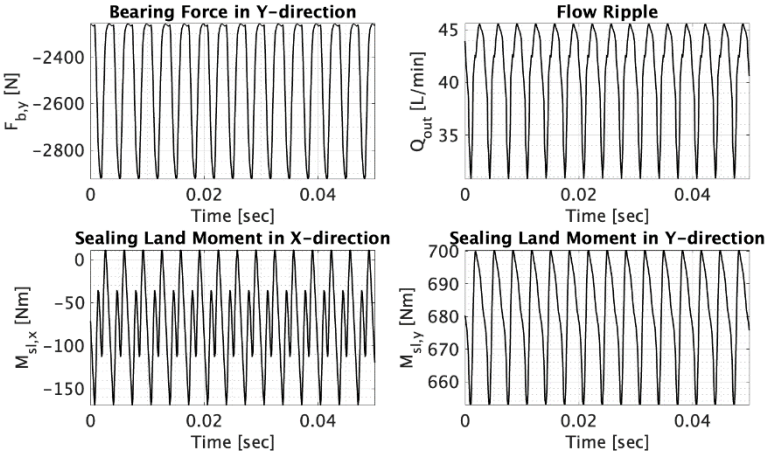

Figure 14 LPM simulation results of excitations. Operation condition: 300 bar, 50% swashplate angle, configuration B.

Due to the cyclic nature of pump operation, Fourier coefficients of both simulation and experiment data are estimated. The phase difference between simulated excitations (**Figure**

14) and sound and vibration measurement results (**Figure 13**) are estimated and compensated by introducing appropriate time delay to the results.

The FRF estimated using sTPA are shown in **Figure 15**. The colour indicates the magnitude of FRF in term of dB. Each value in **Figure 15** indicates the magnitude of noise or vibration caused by a unit of excitation. It can be noticed that the magnitude of FRF's take larger values at higher frequencies. However, larger magnitude of FRF does not necessarily mean the noise and vibration is more significant at particular frequencies. Because the excitations have dominant components at the frequency of piston passage (302 Hz in present study), the spectrum of noise and vibration is also dominated by the components at 302 Hz.

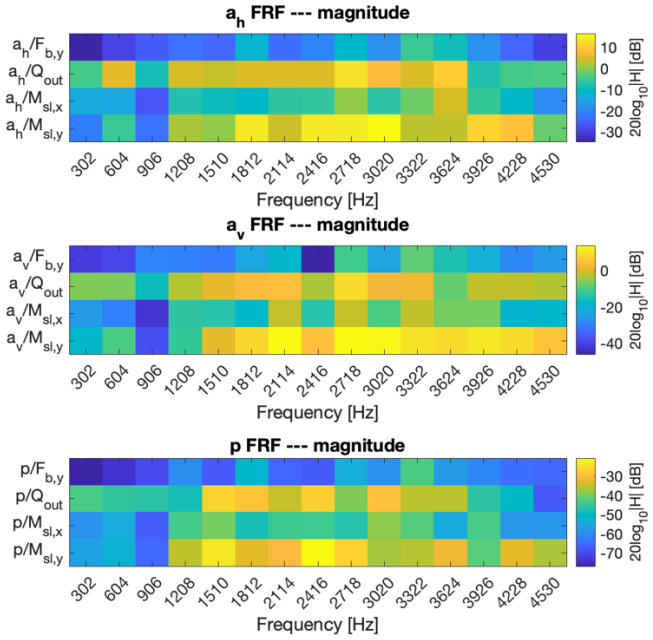

Figure 15 Frequency response functions between excitations ($F_{b,y}$, $M_{sl,x}$, $M_{sl,y}$ and Q_{out}) and responses (a_h, a_v and p).

4.1. Path Contribution

In order to analyse the root-cause of noise and vibration of piston pumps, path contributions are calculated using FRF estimated using sTPA. For the k-th operation condition, path contribution of the j-th excitation to the i-th response is simply $H_{ij}F_j^{(k)}$. The synthesized response is the summation of all the path contributions, that is, $a_i^{(k)} = \sum_{j=1}^{r} H_{ij}F_j^{(k)}$. Path contributions and synthesized responses are complex and can be drawn on complex plane. **Figure 16** shows the path contribution of a operation at piston frequency (302 Hz) as an example. Each solid arrow in the figure represents a contribution from an excitation (bearing force, sealing land moments or flow ripple) to either a vibrational or acoustical response. The solid arrows connect head-to-tail to form the synthesized response. The figure visualizes

the significance of individual transfer paths as well as the cancellation/enhancement between the paths. For instance, in the individual contributions of $F_{b,y}$ and $M_{sl,x}$ to a_h are both significant, yet they cancel against each other because of 130 degrees phase difference. The contributions to a_v, on the other hand, are in phase with each other and contributes evenly to the response. The measurement value is also shown in **Figure 16** for reference. **Figure 17** shows the comparison between synthesized response and measured response in time domain for the corresponding operation condition. The difference between measured response and synthesized response is due to the linear system for H_{ij} being overdetermined.

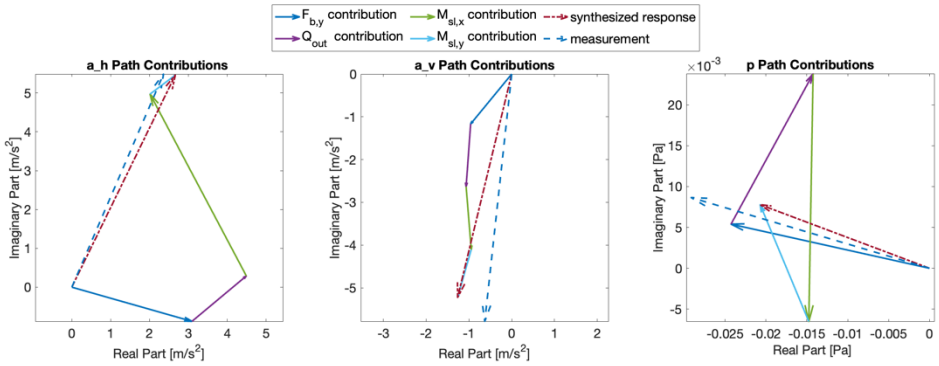

Figure 16 Path contributions. Operation condition: 300 bar, 50% swashplate angle, configuration B. Frequency = 302 Hz.

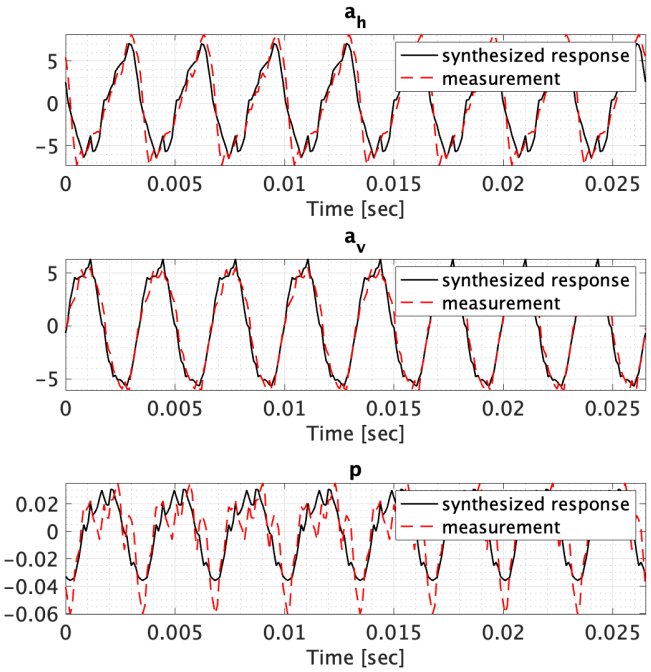

Figure 17 Time domain comparison between synthesized response and measurement.

4.2. Sensitivity analysis

Sensitivity analysis can be conducted based on the information of path contributions. In this study, the sensitivity of noise and vibration responses to excitation magnitudes are analysed. The overall sound pressure or acceleration level is used as the metric of noise/vibration performance of the pump. The overall level of the i-th response is calculated as

$$OL_i = 20\log_{10}\frac{a_{i,rms}}{a_{i,ref}},$$
$$a_{i,rms} = \frac{1}{n}\sum_{k=1}^{n}\sqrt{\sum_{l=-N_f}^{N_f}\left|a_i^{(k)}(f_l)\right|^2}. \tag{11}$$

$a_{i,ref}$ is the reference value for the i-th response and its value is 10 μm/s^2 and 20 μPa for acceleration and sound pressure respectively.

The sensitivities of the three responses (a_h, a_v and p) to the magnitude of the four excitations ($F_{b,y}$, $M_{sl,x}$, $M_{sl,y}$ and Q_{out}) are shown in **Figure 18** The magnitude of each excitation is set to independently vary over a ±20% range (the change of one excitation does not affect other excitations), and the overall levels of synthesized responses are evaluated. The red dashed lines in the figures indicate the reference point. As shown in the figure, all the curves are monotonically increasing, which implies the positive correlation between force/moment/ripple excitations and noise/vibration responses. The figure also indicates potentials of noise and vibration control. For example, overall sound pressure level can be decreased by 0.55 dB if the oscillations in bearing force decreases by 20%, overall horizontal acceleration decreases by 0.61 dB if X-moment oscillation decreases by 20%. Similar analysis can be conducted for excitation phase.

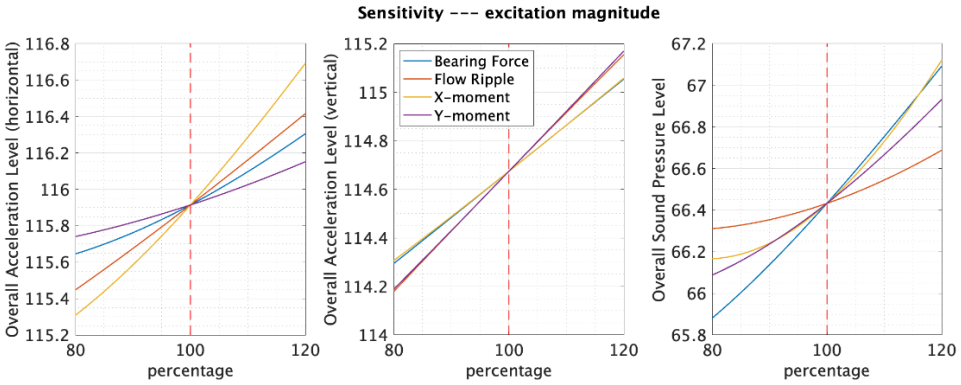

Figure 18 Sensitivity of noise and vibration response to excitation magnitudes.

A further comment on the generality of the sensitivity analysis needs to be emphasized. In such analysis, it is assumed that the transfer paths are not altered as parameters vary. For example, the graph shown in **Figure 18** can be interpreted as predictions of pump noise and vibration, only if the magnitude of excitations can increase/decrease without changing the characteristics of transfer paths. On the other hand, if the change of parameter is associated

with change in pump design, the parameter sensitives is not predictive, and sTPA can only be seen as an additional analysis to close the gap between LPM simulation and pump NVH.

5. CONCLUSION

sTPA is a tool that bridges the gap between LPM calculation results and air-borne noise/vibration performance of hydraulic pumps and provides insights to the root-cause of noise and vibration problems of axial piston pumps. The FRF estimated via sTPA indicates the quantitative relation between internal excitations (forces, moments, ripples etc.) calculated in LPM and consequent noise and vibration. Path contributions estimated in sTPA demonstrate how different sources of noise and vibration add up to the overall noise and vibration effect of the pump and highlights the most significant noise/vibration contributor. Based on the sensitivity analysis of sTPA, the potential pump noise/vibration control measures can be evaluated in terms noise/vibration level decrement.

6. REFERENCES

[1] Schleihs, C. (2017). Acoustic Design of Hydraulic Axial Piston Swashplate Machines. *Reihe Fluidtechnik*, 89. RWTH Aachen University.

[2] Helgestad, B. O., Foster, K. and Bannister, F. K. (1974). Pressure transients in an axial piston hydraulic pump. *Proceedings of Institution of Mechanical Engineers*. 188(1):189-199.

[3] Yamauchi, K. and Yamamoto, T. (1976). Noises generated by hydraulic pumps and their control method. *Mitsubishi technical review*, 13(1).

[4] Kim, T. and Ivantysynova, M. (2017). Active Vibration Control of Swash Plate-Type Axial Piston Machines with Two-Weight Notch Least Mean Square/Filtered-x Least Mean Square (LMS/FxLMS) Filters. *Energies*. 10(5):645.

[5] Harrison, A. M. and Edge, K. A. (2000). Reduction of axial piston pump pressure ripple. *Proceedings of Institution of Mechanical Engineers*, *Part I: Journal of Systems and Control Engineering*. 214(1):53-64.

[6] Ortwig, H. (2005). Experimental and analytical vibration analysis in fluid power systems. *International Journal of Solids and Structures*. 42:5821-5830.

[7] Rebel, J. (1977). Active liquid noise-suppressions in oil hydraulics. *VDI-Z*. 119:937-943.

[8] Manco, S., Nervegna, N., Lettini, A. and Gilardino, L. (1999). An experience in simulation: the case of a variable displacement axial piston pump. *JFPS International Symposium on Fluid Power.*

[9] Manco, S., Nervegna, N., Lettini, A. and Gilardino, L. (2002). Advances in the simulation of axial piston pumps. *JFPS International Symposium on Fluid Power*.

[10] Ivantysyn, J. and Ivantysynova, M. (2001). *Hydrostatic pumps and motors*.

[11] Van der Seijs, M., de Klerk, D. and Rixen, D. (2015). General framework for transfer path analysis: History, theory and classification of techniques. *Mechanical Systems and Signal Processing*. 68-69: 217-244.

[12] de Klerk, D. and Ossipov, A. (2010). Operational transfer path analysis. *Mechanical Systems and Signal Processing*. 24: 1950-1962.

[13] de Sitter, G., Devriendt, C., Guillaume, P. and Pruyt, E. (2010). Operational transfer path analysis. *Mechanical Systems and Signal Processing*. 24: 416-431.

[14] Roozen, N. B. and Leclère, Q. (2013). On the use of artificial excitation in operational transfer path analysis. *Applied Acoustics*. 74: 1167-1174.

[15] Sievi, A., Martner, O. and Lutzenberger, S. (2013). Noise Reduction of Trains Using the Operational Transfer Path Analysis – Demonstration of the Method and Evaluation by Case Study. In: Maeda, T., et al. Noise and Vibration Mitigation for Rail Transportation Systems. *Notes on Numerical Fluid Mechanics and Multidisciplinary Design*, vol 118. Springer, Tokyo.